RSC Advances

PAPER

View Article Online
View Journal | View Issue

Cite this: *RSC Adv.*, 2020, **10**, 9539

Theoretical study on NO_x adsorption properties over the α-MnO_2(110) surface

Xingguang Hao,[a] Xin Song,[a] Kai Li,[a] Chi Wang,[b] Kunlin Li,[a] Yuan Li,[a] Xin Sun *[a] and Ping Ning *[ac]

Received 13th November 2019
Accepted 29th January 2020

DOI: 10.1039/c9ra09455e

rsc.li/rsc-advances

Herein, α-MnO_2 was studied as an adsorbent for the removal of NO_x (NO, NO_2) derived from flue gas. First-principles calculations based on the density functional theory (DFT) were performed to investigate the NO_x adsorption properties over the α-MnO_2(110) surface. NO strongly adsorbed over the α-MnO_2(110) surface *via* chemisorption spontaneously under 550 K. The NO_2 molecules adsorbed over the surface *via* chemisorption and physisorption when the terminal N- and O atoms approached the surface, respectively. The joint adsorption of NO_x was more stable than the isolated adsorption system. Furthermore, the net charge was transferred from the molecule to the surface. The surface and temperature affected the entropy, enthalpy, NO adsorption and NO_2 desorption in the temperature range of 300–550 K. The equilibrium constants decreased with an increase in temperature, which reduced the conversion rate.

1. Introduction

More than 90% of the total emissions of nitrogen oxides (NO_x) originate from stationary sources (copper smelter off-gas, power plants, *etc.*)[1–4] due to the burning of coke under high-temperature combustion conditions. The spread of NO_x in the atmosphere can lead to a global disaster, including ozone depletion, acid rain, photochemical smog and greenhouse effects.[5,6] Thus, the removal of these contaminants in compliance with environmental emission standards is necessary. NO and NO_2 are the main monitoring objects, which typically make up the total emission of NO_x from industries.[7,8] So far, many methods for controlling NO_x contamination, including SCR (selective catalytic reduction) in the gas phase, absorption in the liquid phase and adsorption in the solid phase, have been developed and applied in industries.[9–11] However, the leakage of NH_3 causes air pollution in SCR methods and produces a large amount of wastewater and results in an increase in cost in absorption methods. Comparing the two above-mentioned methods, adsorption is better for the removal of NO_x owing to its excellent characteristics of larger surface area, better selectivity, higher adsorption capacity and rate, better regeneration, and chemical stability. The sorbents CuO, SnO_2, CeO_2, Al_2O_3, TiO_2, and V_2O_5 have been chosen as the ideal materials to remove NO_x in industries.[12–15] However, the high cost of these noble metal oxides limits their application; therefore, there is a need to find inexpensive materials to remove NO_x efficiently. Chen *et al.* found that α-MnO_2 exhibits the highest adsorption capacity for NO_x among the α-, β-, γ- and σ-MnO_2 phase structures and the abovementioned sorbents.[16] Therefore, α-MnO_2 can act as a suitable sorbent to reduce NO_x emissions. However, very little is known about the NO_x adsorption mechanism over the α-MnO_2 surface. Thus, it is necessary to understand the mechanism with the density functional theory (DFT).

Cockayne *et al.* computed the atomic, electronic, and magnetic properties of α-MnO_2 crystals using the DMol^3 package in Materials Studio to provide quantitative predictions.[17] DFT calculations were performed using the above-mentioned package to investigate the α-MnO_2(110) surface by Liu *et al.*, and the hydroxyl α-MnO_2(110) surface was also simulated with reasonable changes from the crystal structure.[18] For oxygen-rich and oxygen-lean α-MnO_2(110) surfaces, Tang *et al.* explored the surface structure sensitivity of manganese oxides for low-temperature SCR methods to remove NO using the DMol^3 package.[19,20] Thus, herein, the DMol^3 package in Materials Studio was used to simulate a process of NO_x adsorption over the α-MnO_2(110) surface.

This study was aimed at investigating the adsorption mechanism and fundamental chemical reactivity of NO_x over the α-MnO_2 (110) surface based on DFT. The thermodynamic properties (Gibbs free energy change, enthalpy, entropy and equilibrium constant), adsorption properties (adsorption energy) and electronic transfer properties (Mulliken charge) were evaluated to determine the optimal adsorption site over

[a]*Faculty of Environmental Science and Engineering, Kunming University of Science and Technology, Kunming 650500, PR China. E-mail: sunxin_kmust@163.com; ningpingkmust@163.com; Fax: +86-871-65920507; Tel: +86-871-65920507*

[b]*Faculty of Chemical Engineering, Kunming University of Science and Technology, Kunming 650500, PR China*

[c]*National-Regional Engineering Center for Recovery of Waste Gases from Metallurgical and Chemical Industries, Kunming University of Science and Technology, Kunming 650500, PR China*

the (110) surface. Moreover, the potential energy diagrams of the different pathways for NO_x adsorption over the surface were presented and the joint adsorption and analysis temperature effect on the equilibrium constant of NO_x was calculated.

2. Computational method and models

In this research, all calculations were performed with DFT using periodic boundary conditions.[21–24] All DFT calculations were completed using DMol^3 with the GGA (generalized gradient approximation) scheme and PBE (Perdew, Burke and Ernzerhof) exchange-correlation functional to describe the exchange-correlation effects.[18,19] Atomic basis sets were applied numerically in terms of the double numerical plus polarization function (DNP) basis set version 3.5 and a global orbital cutoff of 4.7 Å was applied. The geometry optimization convergence tolerances of the energy, gradient, and displacement were 1×10^{-5} Hartree (Ha), 2×10^{-3} Ha Å^{-1}, and 5×10^{-3} Å, respectively. The core electrons were modeled using a density functional semi-core pseudopotential (DSPP) method for Mn atoms, and the all-electron method was used for the core electrons of the N and O atoms. For bulk lattice optimization, energies were converged with $(3 \times 3 \times 9)$ k points in a Monkhorst–Pack grid. The crystal structure of the optimized α-MnO_2 is shown in Fig. 1a, which is a body-centered tetragonal lattice type with the space group $I4/m$ and its optimized unit cell parameters ($a = b = 9.815$ Å, $c = 2.847$ Å) within +0.67% and −0.49% error of the experimentally determined lattice constants,[25] indicating that the calculation results are reliable.

The α-MnO_2(110) surface was the most thermodynamically stable bulk termination and catalytically active surface.[21,26] Therefore, the calculation of the thermodynamic properties and adsorption energies was performed using the α-MnO_2(110) surface. The surface slab was cleaved from the optimized structure of α-MnO_2. 8 layers of atoms were extracted. The $p(1 \times 1)$ supercell was built with a vacuum region of 15 Å along the z-axis, which is shown in Fig. 1b and c. The Monkhorst–Pack k point sampling was set as $3 \times 3 \times 1$.[18,27] The SCF tolerance and number of cycles were 1.0×10^{-6} Ha and 1000, respectively. In the region of the surface, there were four different types of coordinative oxygen atoms, where the first layer oxygen atom O_f lies on the top of the surface, the O_s atom lies on the second layer oxygen atom, the O_t atom lies on the fifth layer oxygen atom and the O_h atom lies on the sixth layer oxygen atom. The third- and seventh-layer atoms were Mn atoms, which could be chosen as an adsorption position. They were named Mn_f and Mn_s, respectively. The atoms in the region were all relaxed, as shown in Fig. 1d. All the structures were optimized at the same level of theory.

3. Results and discussion

To investigate the stability of the NO_x molecules adsorbed over the α-MnO_2(110) surface, the adsorption energy (E_{ads}) was calculated according to eqn (1).

$$E_{ads} = E_{surf-gas} - E_{surf} - E_{gas} \quad (1)$$

where E_{surf} refers to the total energy of the surface model cleaved after the geometry optimization, E_{gas} refers to the total energy of each NO_x in the gaseous phase after the geometry optimization, and $E_{surf-gas}$ refers to the total energy of the surface-gas supersystem build after the geometry optimization. According to this definition, a positive value, corresponding to an exothermic process, means a stable adsorption system.

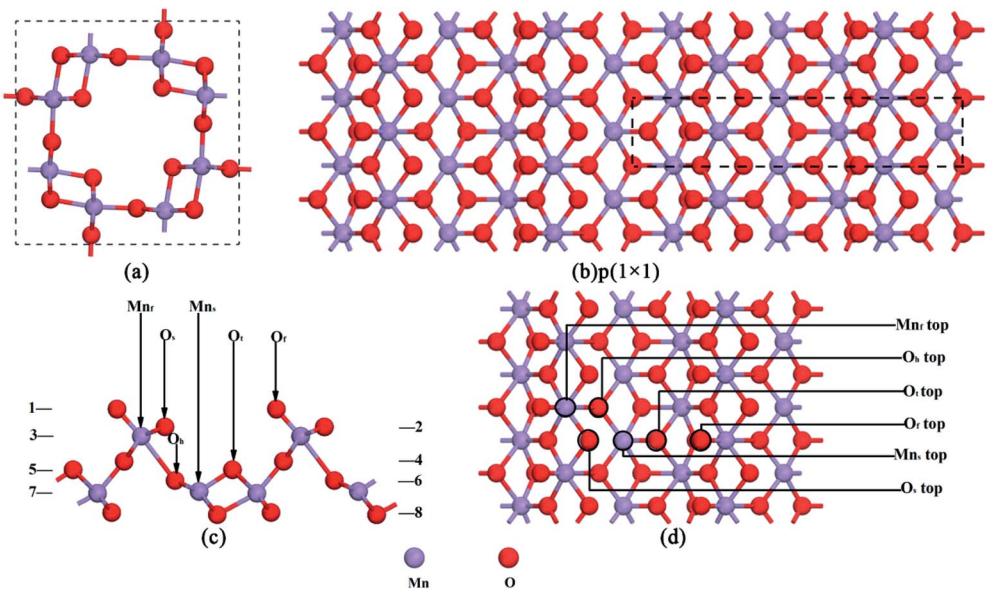

Fig. 1 (a) Optimized α-MnO_2 crystal structure. (b) α-MnO_2(110) surface configuration. (c) Side view of the α-MnO_2(110) surface with eight layers. (d) Top view of the α-MnO_2(110) surface with different adsorption positions.

Moreover, to determine the exothermicity of the adsorption process and to investigate the favorability of the spontaneous reaction as a function of temperature, the equilibrium constant (K_{eq}),[28–32] Gibbs free energy change, entropy (S) and enthalpy (H) were calculated according to the thermodynamic data from the frequency. The general relationships for the statistical thermodynamic partition functions (translational, rotational, and vibrational partition functions) were introduced.[33] The equilibrium constant (K_{eq}) can be defined as eqn (2).

$$\ln(K_{eq}) = -\Delta G/RT \quad (2)$$

where ΔG refers to the Gibbs free energy change, R refers to the ideal gas constant, and T refers to the temperature. According to this definition, the greater the equilibrium constant, the more thorough the reaction.

The Gibbs free energy change during the adsorption process was calculated using eqn (3).

$$\Delta G \approx \Delta E_{ads} + \Delta E_0 + T(\Delta S_{vib} + \Delta S_{trans,rot}) - kT \ln\left(\frac{P}{P_0}\right) \quad (3)$$

where ΔE_{ads} refers to the change in adsorption energy, ΔE_0 refers to the change in the zero-point energy, and ΔS_{vib} and $\Delta S_{trans,rot}$ refer to the changes in the vibrational and translational, rotational entropy during adsorption, respectively.[33] k refers to the Boltzmann constant, and the pressure terms were canceled out because the pressure was constant in this adsorption system. The above equations were used to obtain ΔG and K_{eq} for NO_x adsorption in the temperature range of 200–1000 K, which covers most experimental relevance for real adsorption systems. According to this definition, a negative value of ΔG means a spontaneous process for NO_x adsorption.

The net charge-transfer (Q) was calculated using eqn (4).

$$Q = \text{Mulliken charge}_{after} - \text{Mulliken charge}_{before} \quad (4)$$

where Mulliken charge$_{after}$ refers to the Mulliken charge of the NO_x molecule in the adsorbed state, and Mulliken charge$_{before}$ refers to the Mulliken charge of the NO_x molecule in the gaseous phase. According to this definition, a positive value means a loss of electrons from the NO_x molecule.[34]

The heat (Q) that an adsorption system adsorbs at a specific temperature was calculated using eqn (5).

$$Q = nC_{p,T}T \quad (5)$$

where n refers to the amount of substance. $C_{p,T}$ refers to the heat capacity at a constant pressure and specified temperature.

The entropy value (S) was calculated using eqn (6).

$$S = Q/T \quad (6)$$

The enthalpy value (H) was calculated using eqn (7).

$$H = U + pV \quad (7)$$

where U refers to the internal energy, p refers to the pressure and V refers to the volume.

3.1 Adsorption of NO molecule over the α-MnO_2(110) surface

Deshwal *et al.* found that the major component of NO_x was NO (*ca.* 90%) in flue gas.[35] Also, NO was found to be an intermediate in the industrial production of nitric acid.[36,37] Therefore, it is important to investigate the NO adsorption mechanism over the α-MnO_2(110) surface to remove the vast majority of NO_x as a raw material for the production of nitric acid. Before adsorption, the bond length of the free NO molecule was calculated to be 1.163 Å, which is close to the experimental value (1.17 Å).[38,39] Then, an isolated adsorption system is formed, and the NO molecule adsorbs over the different adsorption positions of the α-MnO_2(110) surface. The optimized models of NO adsorption are presented in Fig. 2. The adsorption energies, bond length, distance and net charge-transfer for NO adsorption over the α-MnO_2(110) surface are shown in Table 1.

As shown in Table 1, the adsorption strength for NO adsorption over the surface followed the order of 2C < 2F < 2A<2D < 2E < 2B. This indicates that all the NO adsorption sites exhibited chemisorption, suggesting an exothermic process and a stable adsorption system. The NO molecule adsorbed over the surface is chemisorption, which was modeled by attaching the molecule to the surface by its N atom as well as by its O atom. In the adsorption process, the net charge-transfer based on the Mulliken population analysis was investigated to determine the charge-transfer mechanism between the molecule and surface. The results presented in Table 1 show that the adsorbed NO molecule was positively charged on all the models. This means that electrons transfer from NO to the surface, which indicates that NO acts as a donor to provide electrons. The reason for this that the electronic arrangement of the N and O of NO is $2s^2p^3$ and $2s^22p^4$, respectively, and they form polar covalent bonds *via* sp hybridization. The hybridization of the atomic orbital of N and O forms a σ bond, a 2-electron π bond and a 3-electron π bond among the polar covalent bonds. There is a lone-pair of electrons in the 2p orbitals of the N atom and also the O atom. Besides, the Mulliken charge was easily affected by the basis set. Hence, there is a lone-pair of electrons from the 2p orbitals with an unpaired electron to be filled in the surface, which is influenced by the basis set. Moreover, the optimized bond lengths of the adsorbed NO molecule in the equilibrium state were all shorter than that in the free case, illustrating that the surface makes the molecule more stable and it is difficult to break the covalent bond after it is adsorbed over the surface. In addition, the optimized distance between the N or O atoms of the adsorbed NO molecule and O or Mn atoms of the surface was probably short enough to form a chemical bond among the NO molecules and the surface. For the six different configurations, it was found that all the distances between the molecule and the surface were less than 3.76 Å,[40] which showed that our calculation was reasonable.

The most stable model is 1B in Table 1, which lies on the Mn_s top site, but approaches the O_s site with both O and N in the N-

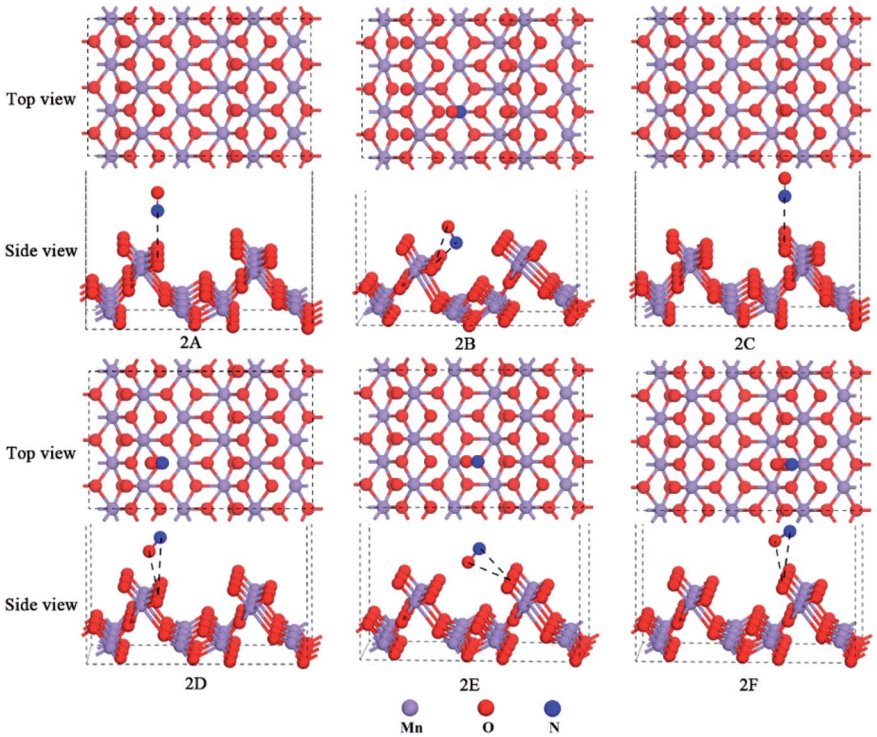

Fig. 2 Optimized models of NO adsorption over the α-MnO_2(110) surface.

down orientation and the distance of 2.592 Å and 1.969 Å, respectively. The adsorption energy was −85.05 kJ mol^{-1}. Combining the bond lengths of NO, the distance between the molecules and the surface was 1.969 Å and 1.127 Å, and thus it can be concluded that the distance between the adsorbed molecules and the surface is due to the formation of chemical bonds. The reason for this that the formed chemical bond will lead to the covalent bond interaction in the adsorbed NO molecule becoming smaller than that in the free NO molecule. This explanation has been already applied to the adsorption of CO molecules on the orthorhombic structure of the $LaMnO_3$(110) surface.[34]

Also, the thermodynamic properties (S, H and ΔG) as a function of temperature were calculated and DMol^3 was used to plot the thermodynamic properties, as shown in Fig. 3. Furthermore, all the data for NO were demonstrated to be reliable compared to the experimental data.[41] In Fig. 3a, the entropy values of all the configurations increase and their growth rate decrease when NO was almost parallel to the x-axis compared to the other configurations within the range of 44.92 to 56.63 cal mol^{-1} K as the temperature increased. As calculated using eqn (5) and eqn (6), the blue line in Fig. 3a and c should be parallel, but it is not and also the red line. This is because of the conversion of exergy and heat caused by increasing the temperature in the system. Obviously, exergy has a greater influence on entropy. Due to the stability of the NO molecule in the gaseous phase, it has a stable heat capacity and its covalent bond never breaks in the temperature range of 200–1000 K parallel to the x-axis. Also, the values for the NO adsorption system of Model 2B (S_{ads}) were higher than that in the other conditions and close to the values of the α-MnO_2(110) surface (S_{surf}) at the same temperature, and the gap between the surface and the adsorption system increased with an increase in temperature. This indicates that the entropy of the adsorption system is affected more by the surface than by the NO molecule with a change in temperature and makes the molecule unstable to leave the surface. Also, we found that $S_{ads} < S_{surf} + S_{NO}$ and the value of $S_{ads} - S_{surf}$ was lower in the range of 33.37–33.95 cal mol^{-1} K^{-1} compared to S_{NO} (44.92–56.63 cal mol^{-1} K). This indicates that the NO molecule binds on the surface stably and does not undergo desorption and dissociation. In Fig. 3b, the growth rate and enthalpy values of the adsorption system and the surface increase and are close to each other when the free NO molecule is almost parallel to the x-axis with a positive

Table 1 The adsorption energies, bond lengths, distances and net charge-transfer for NO adsorption over the α-MnO_2(110) surface[a]

Model	E_{ads}	L_{N-X}	L_{O-X}	$d_{N=O}$	Q_{NO}
2A	−53.97	3.014	—	1.131	0.34
2B	−85.05	1.969	2.592	1.127	0.41
2C	−48.65	3.012	—	1.133	0.31
2D	−56.42	3.699	2.863	1.128	0.35
2E	−63.93	2.869	2.928	1.124	0.38
2F	−53.53	3.290	2.727	1.130	0.33

[a] E_{ads} is the adsorption energies (kJ mol^{-1}); L_{N-X} is the distance between N of the adsorbed NO molecule and closest adsorbate atom (Å); L_{O-X} is the distance between O of the adsorbed NO molecule and closest adsorbate atom (Å); $d_{N=O}$ is the bond length of the adsorbed NO molecule; and Q_{NO} is the net-charge transfer of the NO molecule (e).

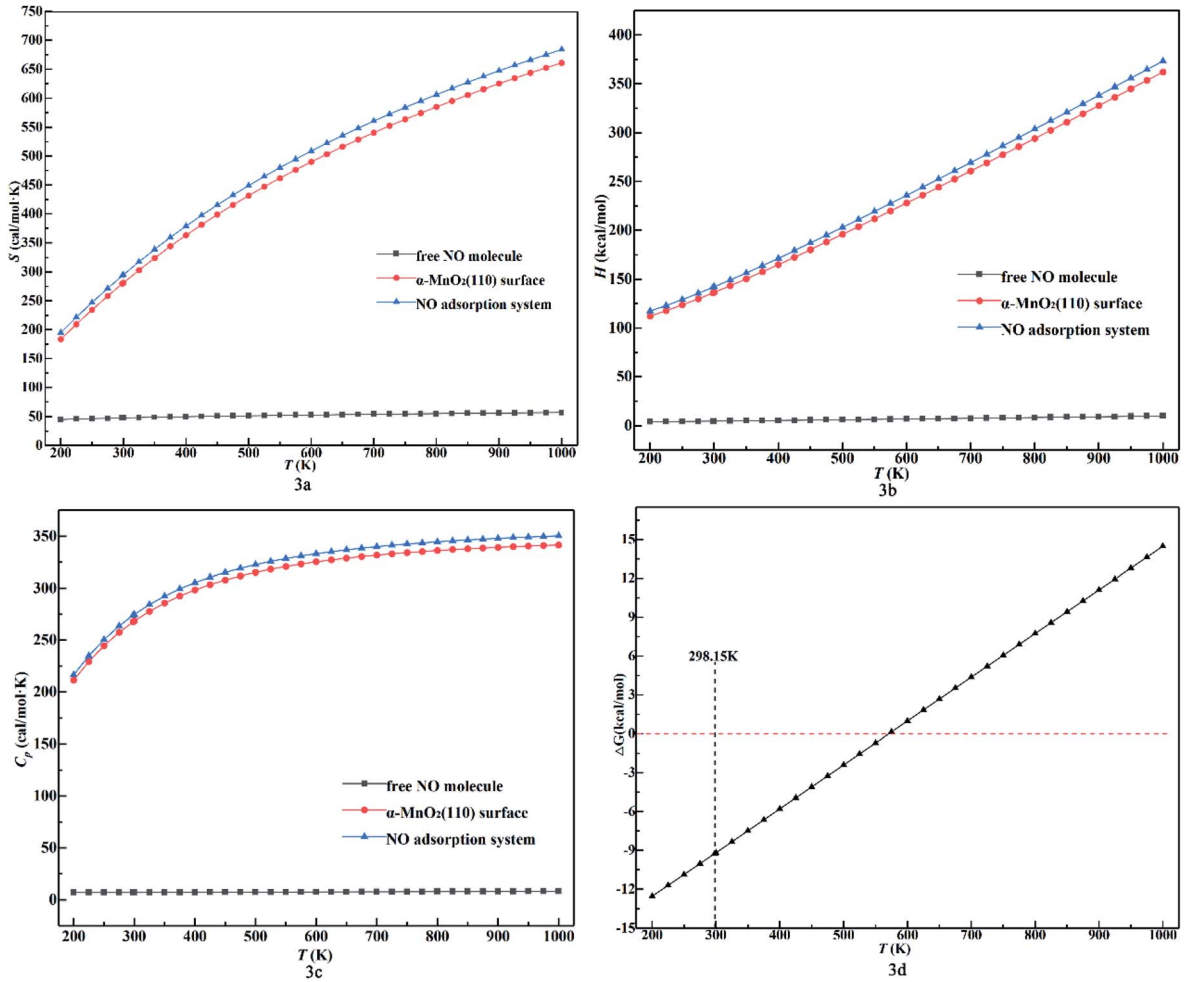

Fig. 3 (a) Entropy value. (b) Enthalpy value. (c) Heat capacity value and (d) Gibbs free energy change for NO adsorption system of Model 2B as a function of temperature (kcal mol^{-1}) (the black dashed line represents temperature of 298.15 K, and the red dashed line represents ΔG of 0).

increase in temperature. This indicates that all the configurations are endothermic and the enthalpy of the adsorption system is mainly affected by the surface clearly with an increase in temperature. Besides, the enthalpy was calculated using eqn (7), which is approximately equal to the heat at a constant pressure. Thus, it is influenced by heat, which is a function of temperature, and the heat capacity to cause the rate to increase. Meanwhile, heat in the phase transition does not occur in the adsorption system, as reflected in Fig. 3b by the slight changes in the enthalpy value in the range of 200–1000 K. The phenomenon that the distance between the adsorption system and the surface increases with an increase in temperature reveals that the adsorption system will adsorb more heat than the surface. In Fig. 3d, the plot of ΔG shows an increasing trend with negative values under 550 K and finally becomes positive with an increase in temperature. This indicates that the system functions spontaneously under 550 K and is suitable for laboratory experiments.[42–44] Finally, we calculated the thermodynamic properties at 298.15 K, including $H = 293.36$ cal mol^{-1} K, $S = 141.86$ kcal mol^{-1}, $\Delta G = -9.25$ kcal mol^{-1}, and $C_p = 274.14$ cal mol^{-1} K^{-1}. This indicates that at room temperature, the reaction is spontaneous.

The potential energy diagram for the different pathways of NO adsorption over the (110) surface including the reactants, intermediates and products is shown in Fig. 4. The energies of

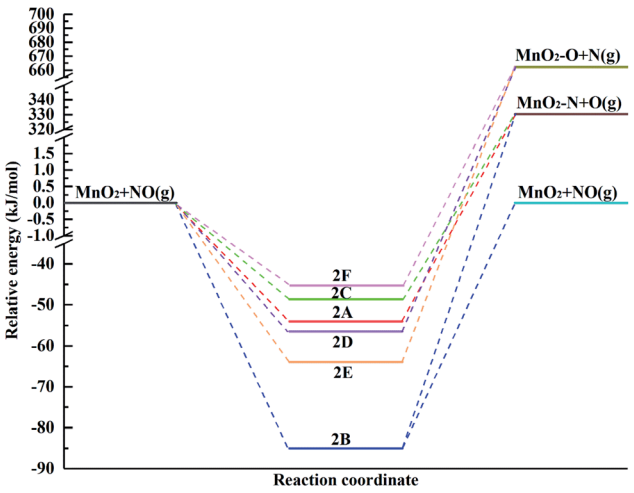

Fig. 4 Potential energy diagram for the different pathways for the adsorption of the NO molecule over the α-MnO_2(110) surface.

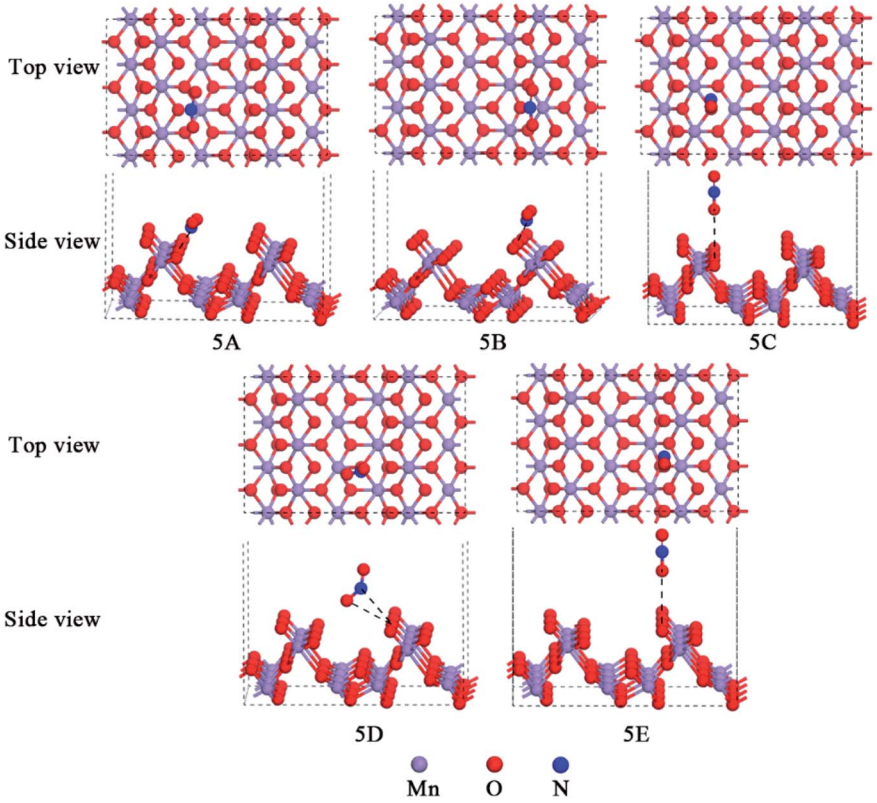

Fig. 5 Models of NO_2 adsorption over the α-MnO_2(110) surface after optimization.

the optimized structures were relative to the reactants. The desorption of the NO molecule is highly endothermic by 85.05 kJ mol^{-1}, and its dissociation, *i.e.*, N adsorption over the surface and O desorption, is highly endothermic by 384.34 kJ mol^{-1}, 415.42 kJ mol^{-1} and 379.02 kJ mol^{-1} for 2A, 2B and 2C, respectively (the adsorption orientation in the N-down mode), while O adsorption over the surface and N desorption are highly endothermic by 718.60 kJ mol^{-1}, 726.12 kJ mol^{-1} and 715.72 kJ mol^{-1} for 2D, 2E and 2F, respectively, in the case of the O-down mode. This means that NO prefers to adsorb over the surface rather than dissociate due to the higher energy required to break the covalent bond and lower adsorption energy after geometry optimization of the dissociation model. If an NO molecule was dissociating, it will receive priority in binding N over the surface. Therefore, once NO adsorbs over the surface, it will neither easily desorb nor dissociate from the surface.

3.2 Adsorption of NO_2 molecule over the α-MnO_2(110) surface

NO_2 is reddish-brow toxic gas, which can act as a raw material in the nitric acid industry.[45,46] The parameters for the free NO_2 were calculated to be $d_{N-O} = 1.211$ Å, $d_{N=O} = 1.211$ Å, and $\theta_{NO_2} = 132.95°$, in good agreement with that by Greenwood *et al.*[47] The interactions of NO_2 with different active sites of the α-MnO_2(110) surface were studied. Several possible models of NO_2 molecule adsorption over the α-MnO_2(110) surface were built and then geometry optimization was performed to determine the optimum model. Besides, the adsorption of NO_2 was modeled by attaching the molecule to the surface by its terminal N atom and by its terminal O atom vertically. After geometry optimization, the stable configurations of NO_2 over the α-MnO_2(110) surface are presented in Fig. 5 and Table 2 exhibits the adsorption energies, bond lengths, distance between the NO_2 molecule and the surface, bond angles and net charge-transfer for NO_2 adsorption over the α-MnO_2(110) surface. It was found that the most stable configuration for NO_2

Table 2 The adsorption energies, bond lengths, bond angles, distances and net charge-transfer for NO_2 adsorption over the α-MnO_2(110) surface[a]

Model	E_{ads}	L_{N-X}	L_{O-X}	θ_{NO_2}	d_{N-O}	$d_{N=O}$	Q_{NO_2}
5A	−69.74	2.335	—	135.44	1.192	1.192	0.26
5B	−56.81	1.829	—	135.78	1.193	1.195	0.25
5C	−14.98	—	3.355	137.44	1.197	1.200	0.17
5D	−20.05	3.097	3.172	138.67	1.194	1.196	0.21
5E	−13.08	—	3.365	136.98	1.198	1.201	0.15

[a] E_{ads} is the adsorption energy (kJ mol^{-1}); L_{N-X} is the distance between N of the adsorbed NO_2 molecule and closest adsorbate atom (Å); L_{O-X} is the distance between O of the adsorbed NO_2 molecule and closest adsorbate atom (Å); d_{N-O} and $d_{N=O}$ are the bond lengths of the NO_2 molecule after adsorption (Å); Q_{NO_2} is the net-charge transfer of the NO_2 molecule (e); and θ_{NO_2} is the bond angle of the adsorbed NO_2 molecule (°).

over the surface is 5A, which is on a hollow site that is surrounded by Mn_s and O_h but approaches O_s the closest, and its adsorption energy of -69.74 kJ mol^{-1} indicates chemisorption *via* the N-terminal approaching the surface. In contrast, 5D was physisorption with -20.05 kJ mol^{-1} *via* the O-terminal approach, with the approach of the closest O_f, which is the most stable model on the Mn_s–O_t bridge site in the physical adsorption process. Also, the angle increases from 132.95° to 135.44° and the bond lengths decrease from 1.211 Å to 1.192 Å in the chemisorption process, while the angle increases to 138.67° and the bond lengths decrease to 1.194 Å and 1.201 Å. This can be influence by the net-charge transfer and adsorption energy. The former indicates that the surface is a receiver of charge from the molecule and that the NO_2 molecule forms covalent bonds with an unpaired electron from the 2p orbitals of O and N.

It is important to investigate the chemisorption and physisorption for NO_2 adsorption over the surface and determine how to influence the properties of the surface based on analysis of the thermodynamic data. Models 5A and 5D were chosen because they are most stable configurations in the process of chemisorption and physisorption, respectively. The temperature and adsorption energy can influence the thermodynamic data. Thus, the DMol^3 thermodynamic properties as a function of temperature was plotted, as shown in Fig. 6. In Fig. 6a, the entropy value increases while its growth rate decreases. Also, with an increase in temperature, the growth rate for chemisorption is higher than that for physisorption initially and lower finally. This indicates that the chemical bond formed during chemisorption between the molecule and the surface changes the reactivity, which is the sensitivity to the desorption of the NO_2 molecule. In Fig. 6b, enthalpy value and its growth rate increases with an increase in temperature and becomes almost parallel for chemisorption and physisorption. This indicates that the adsorption system adsorbs heat with an increase in temperature. Also, the distance between chemisorption and physisorption is caused by the surface activity relative to the adsorption energy. Fig. 6c shows that the Gibbs free energy increases proportionally with respect to temperature for both chemisorption and physisorption. This indicates that ΔG can be influenced by temperature and the adsorption energy. Under 250 K, the physisorption values are higher than 0, while the chemisorption values are lower than 0 at the same temperature. This reveals that the adsorption energy from the

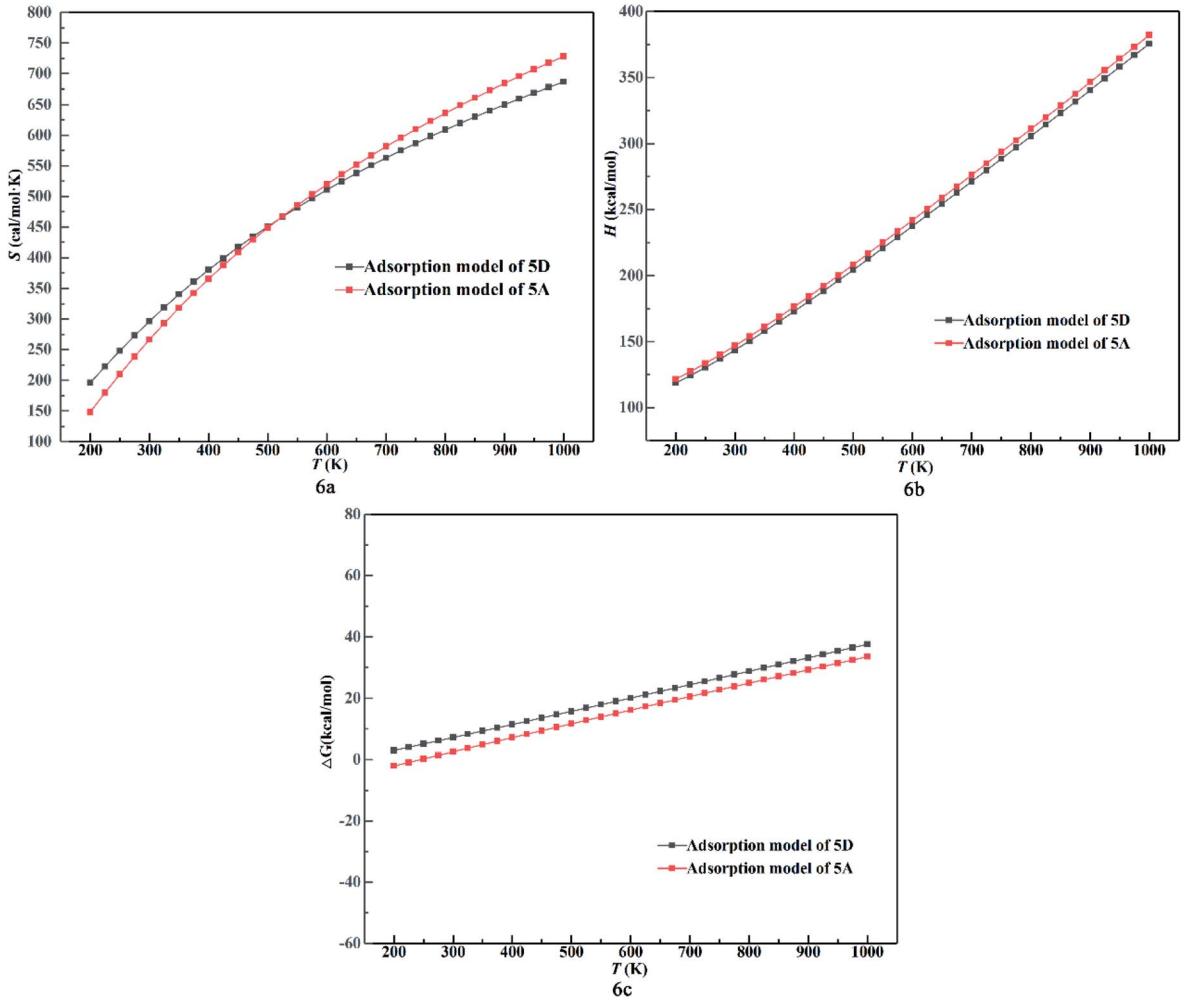

Fig. 6 (a) Entropy value, (b) enthalpy value and (c) Gibbs free energy change of 5A and 5D as a function of temperature.

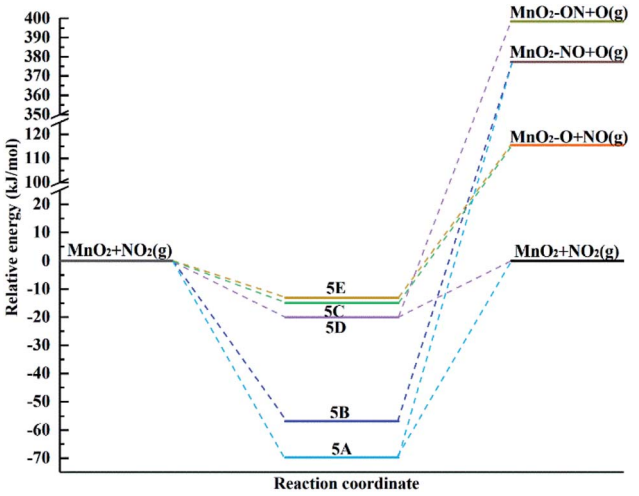

Fig. 7 Potential energy diagram for the different pathways for the adsorption of the NO_2 molecule over the α-MnO_2(110) surface.

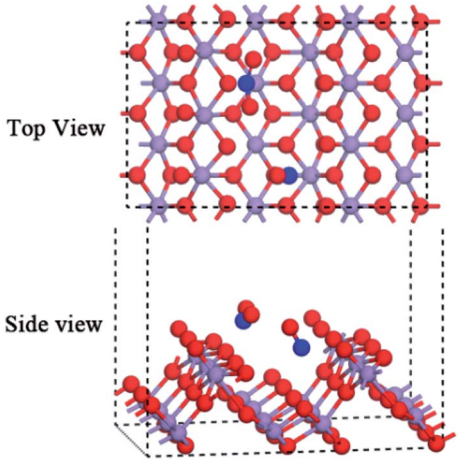

Fig. 8 Joint adsorption of NO and NO_2 over the α-MnO_2(110) surface.

surface influences the reaction to be spontaneous or not at low temperature.

The energy diagram of NO_2 adsorption and possible desorption over the surface including reactants, intermediates and products is shown in Fig. 7. The energies of the optimized structures are related to the reactants. The stability of the surface complex follows the order of 5A>5B > 5D > 5C > 5E. In the chemisorption process, the formation of intermediate 5A and 5D in the physisorption process is highly exothermic, indicating that the surface complexes 5A and 5D are the most likely structures to be formed. In the case of 5A and 5B, they exhibit chemisorption with the formation of a chemical bond between the surface and the molecule. Also, the dissociation of the NO molecule adsorbed over the surface occurs *via* N-down and O desorption, which are highly endothermic by 447.05 kJ mol^{-1} and 434.12 kJ mol^{-1}, respectively, indicating that this cannot occur. 5C, 5D and 5E exhibit physisorption. The process of forming intermediates 5C and 5E leads to NO_2 dissociation of the adsorbed NO *via* O-down and O desorption, which are highly endothermic by 130.54 kJ mol^{-1} and 128.64 kJ mol^{-1}, respectively. Due to the higher adsorption energy for the formation of 5D, it will lead to O adsorption and NO desorption with 418.48 kJ mol^{-1}.

3.3 Joint adsorption and temperature effect on the equilibrium constants of NO_x

The major components of NO_x are NO and NO_2 in flue gas. Hence, it is necessary to determine the mechanism of how NO and NO_2 jointly adsorbed over the surface influence each other that. Previously, the calculated values of $E_{ads\_NO} = -85.05$ kJ mol^{-1} and $E_{ads\_NO_2} = -69.74$ kJ mol^{-1} showed that NO adsorbs over the surface mainly *via* the chemisorption mechanism. As seen in Fig. 8, when NO and NO_2 jointly adsorb over the surface, the adsorption energy is −157.36 kJ mol^{-1}, *i.e.*, the chemisorption effect is enhanced. Also, $d_{N=O} = 1.118$ Å (in NO) and $d_{N-O} = d_{N-O} = 1.202$ Å (in NO_2). In comparison with the isolated adsorption system, the joint adsorption makes NO more stable and NO_2 more vulnerable. Meanwhile, the distance between O (in NO) and O (in NO_2 from the single bond) is 3.307 Å longer than the bond length of the covalent bond, which cannot form a chemical bond between NO and NO_2 in the joint adsorption system. Besides, the joint adsorption energy is higher than the isolated adsorption energy with a value of −2.57 kJ mol^{-1}. This indicates that the adsorption of both NO and NO_2 over the surface will enhance the adsorption effect and improve their stability.

Temperature can influence the conversion rates relate to the equilibrium constants for NO_x adsorption over the α-MnO_2(110) surface. The equilibrium constants for the adsorption of NO, NO_2 and joint adsorption over the α-MnO_2(110) surface in the temperature range of 200–1000 K are shown in Fig. 9. The results indicate that all the adsorption systems have positive slopes in the studied temperature range and the equilibrium

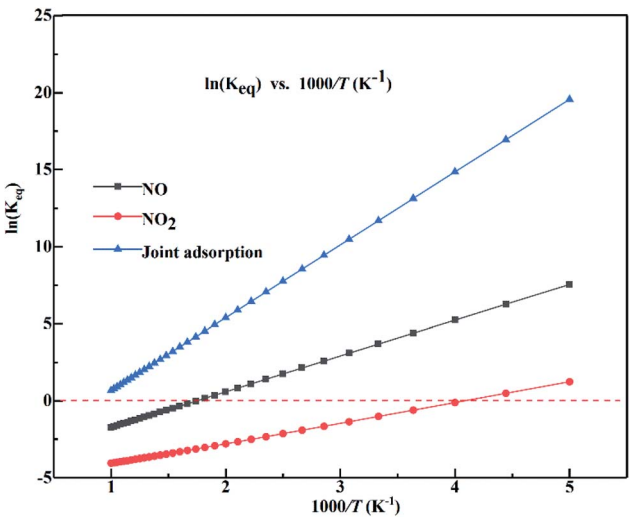

Fig. 9 Equilibrium constants for the adsorption of NO, NO_2 and their joint adsorption over the α-MnO_2(110) surface as a function of temperature (the red dashed line represents ln(K_{eq}) of 0).

increases as the temperature increase. The joint adsorption has the largest slope, indicating that temperature has the strongest effect on the equilibrium constant for joint adsorption. Also, a negative value was obtained for the isolated adsorption, but not for the joint adsorption, indicating that the isolated adsorption system can desorb from the surface at a high temperature, while the joint adsorption can enhance the stability of NO and NO_2 adsorbed over the surface in the temperature range of 200–1000 K. The equilibrium constants of NO and joint adsorption were reduced by 61.32% and 95.81%, respectively, when the temperature increased from 300 K to 550 K, indicating that the adsorption efficiency of the sorbent of α-MnO_2 can decrease greatly at temperatures above 550 K. Moreover, NO_2 adsorbed over the surface is easier to desorb from the surface because of its lowest equilibrium constant at the same temperature. The joint adsorption energy was higher than that of the isolated adsorption system because of the van der Waals force among the molecules.

4. Conclusion

The detailed adsorption mechanism of NO_x over the α-MnO_2(110) surface was firstly investigated *via* a systematic density functional theory study. NO strongly adsorbs over the α-MnO_2(110) surface *via* chemisorption spontaneously. The NO_2 molecule adsorbs over the surface *via* chemisorption and physisorption when its terminal N- and O atoms approach the surface, respectively. Besides, the adsorption energy of NO (-85.053 kJ mol^{-1}) is higher than of NO_2 (-69.741 kJ mol^{-1}), indicating that NO adsorbs over the surface initially. The joint adsorption of NO_x is more stable than the isolated adsorption system at 200–1000 K according to the analysis of the thermodynamic data of H and S. S can be influenced by exergy and heat. H can be influenced by heat, but heat in the phase transition does not occur in the adsorption system. The values of H and S for NO adsorption over the surface can be influenced greater by the surface rather than NO in the chemisorption process. Besides, the adsorption is spontaneous under 550 K according to the analysis of the thermodynamic data of $\triangle G$. In the case of NO_2, the different adsorption mechanisms from the analysis of H, S and ΔG can be explained as follows: a chemical bond can be formed during chemisorption to change the sensitivity of the surface and H can be influenced by the temperature and the surface, which influences ΔG. The potential energy diagram for the different pathways for the adsorption of NO and NO_2 over the α-MnO_2(110) surface showed NO adsorption over the surface and NO_2 desorption in the temperature of 300–550 K. Also, joint adsorption maintained a positive value for the equilibrium constants in the temperature range of 200–1000 K, indicating that joint adsorption is beneficial for the adsorption of more contamination at high temperature. Besides, the equilibrium constants of NO and joint adsorption were reduced by 61.32% and 95.81%, respectively, when the temperature increased from 300 K to 550 K, indicating that the adsorption efficiency of the α-MnO_2 sorbent can decrease greatly at temperatures above 550 K. Hence, it is a better approach to regenerate α-MnO_2-based sorbents that have already adsorbed NO, which oxides to NO_2 and then heats the adsorption system. Besides, NO and NO_2 jointly adsorbed over the surface can remove more NO_x at high temperature.

Conflicts of interest

There are no conflicts to declare.

Acknowledgements

This work was supported by National Key R&D Program of China (2018YFC0213400), National Natural Science Foundation of China (51708266, 51408282 and 21667015), China Scholarship Council (201808535082) and the Analysis and Testing Foundation of Kunming University of Science and Technology.

References

1 J. Li, H. Chang, L. Ma, J. Hao and R. T. Yang, *Catal. Today*, 2011, **175**, 147–156.
2 L. Wei, S. Cui, H. Guo and X. MaCollege, *Mol. Catal.*, 2018, **445**, 102–110.
3 X. Cheng, Z. Cui, L. Contreras, M. Chen, A. Nguyen and B. Zhao, *Jom*, 2019, **71**, 1897–1903.
4 D. Tong, Q. Zhang, F. Liu, G. Geng, Y. Zheng, T. Xue, C. Hong, R. Wu, Y. Qin and H. Zhao, *Environ. Sci. Technol.*, 2018, **52**, 12905–12914.
5 W. Xu, R. Wang, Y. Du, X. Li and X. Xie, *New J. Chem.*, 2019, **43**, 2640–2648.
6 A. Nikokavoura and C. Trapalis, *Appl. Surf. Sci.*, 2018, **430**, 18–52.
7 J. J. Shan, Z. Yuan, S. R. Zhang, Z. Tong, S. Rouvimov and F. Tao, *J. Phys. Chem. C*, 2013, **117**, 8329–8335.
8 S. Wang, L. Zhang, L. Wang, W. U. Qingru, F. Wang and J. Hao, *Front. Environ. Sci. Eng.*, 2014, **8**, 631–649.
9 L. Sun, K. Li, Z. Zhang, X. Hu, H. Tian, Y. Zhang and X. Yang, *Catal. Sci. Technol.*, 2019, **9**, 1602–1608.
10 C. V. Raghunath and M. K. Mondal, *Chem. Eng. J.*, 2017, **314**, 537–547.
11 C. Hu, X. J. Kong, R. Q. Yu, T. T. Chen and X. Chu, *Anal. Sci.*, 2017, **33**, 783–788.
12 G. Xu, Z. Lin, C. He, D. Ma and Z. Lu, *Sens. Actuators, B*, 2015, **221**, 717–722.
13 J. Sun, H. Chen, H. Wu, C. Zhou and H. Yang, *Can. J. Chem. Eng.*, 2019, **97**, 2498–2504.
14 N. R. Jaegers, J. K. Lai, Y. He, E. Walter, D. A. Dixon, M. Vasiliu, Y. Chen, C. Wang, M. Y. Hu and K. T. Mueller, *Angew. Chem.*, 2019, **131**, 12739–12746.
15 D. Ma, Y. Liu, B. Huang, L. Wang and F. Dong, *New J. Chem.*, 2019, **43**, 15161–15168.
16 H. Chen, Y. Wang and Y. Lv, *RSC Adv.*, 2016, **6**, 54032–54040.
17 E. Cockayne and L. Li, *Chem. Phys. Lett.*, 2012, **544**, 53–58.
18 Y. Liu, L. Yu, M. Sun, G. Diao, B. Lan and G. Cheng, *Comput. Theor. Chem.*, 2014, **1031**, 1–6.
19 X. Tang, W. Chao, S. Liang, Q. Cao, B. Hu and Z. Huang, *Appl. Catal., B*, 2011, **101**, 598–605.

20 H. U. Pingping, Z. Huang, W. Hua, G. U. Xiao and X. Tang, *Appl. Catal., A*, 2012, **437–438**, 139–148.
21 G. A. E. Oxford and A. M. Chaka, *J. Phys. Chem. C*, 2011, **115**, 16992–17008.
22 X. Song, L. Sun, P. Ning, C. Wang, X. Sun, K. Li and M. Fan, *New J. Chem.*, 2019, **43**, 10066–10072.
23 S. Xin, N. Ping, W. Chi, L. Kai and S. Xin, *Appl. Surf. Sci.*, 2017, **414**, 345–352.
24 S. Xin, N. Ping, L. Kai, S. Xin, W. Chi and L. Sun, *Chem. Eng. J.*, 2018, **348**, 630–636.
25 J. Luo, C. Hu, X. Meng, J. Crittenden, J. Qu and P. Peng, *ACS Sustainable Chem. Eng.*, 2017, **5**, 2255–2264.
26 G. A. E. Oxford and A. M. Chaka, *J. Phys. Chem. C*, 2012, **116**, 11589–11605.
27 H. J. Monkhorst and J. D. Pack, *Phys. Rev. B: Solid State*, 1976, **13**, 5188–5192.
28 B. Delly, *J. Chem. Phys.*, 2000, **113**, 7756–7764.
29 J. A. W. Elliott and C. A. Ward, *Langmuir*, 1997, **13**, 951–960.
30 K. B. Gyeong, L. Xinxin and B. Paul, *Langmuir*, 2009, **25**, 2781–2789.
31 B. Paul and K. B. Gyeong, *J. Mol. Model.*, 2011, **17**, 505–514.
32 B. Zhang, L. Jing, C. Zheng and C. Ming, *Chem. Eng. J.*, 2014, **256**, 93–100.
33 D. Loffreda, *Surf. Sci.*, 2006, **600**, 2103–2112.
34 C. Shi, L. Sun, H. Qin, X. Wang, L. Ling and J. Hu, *Comput. Mater. Sci.*, 2015, **98**, 83–87.
35 B. R. Deshwal, S. J. Dong, H. L. Si, S. H. Moon, J. H. Jung and H. K. Lee, *J. Hazard. Mater.*, 2008, **150**, 649–655.
36 I. I. Zakharov and B. F. Minaev, *Theor. Exp. Chem.*, 2011, **47**, 93–100.
37 I. I. Zakharov and B. F. Minaev, *J. Struct. Chem.*, 2012, **53**, 1–11.
38 H. Gao and Z. Liu, *RSC Adv.*, 2017, **7**, 13082–13091.
39 M. P. Jigato, K. Somasundram, V. Termath, N. C. Handy and D. A. King, *Surf. Sci.*, 1997, **380**, 83–90.
40 O. Leenaerts, B. Partoens and F. Peeters, *Phys. Rev. B: Condens. Matter Mater. Phys.*, 2008, **77**, 1–6.
41 D. D. Wagman, W. H. Evans, V. B. Parker, R. H. Schumm, I. Har-low, S. M. Bailey, K. L. Churney and R. L. Nuttall, The NBS Tables of Chemical Thermodynamic Properties, *J. Phys. Chem. Ref. Data*, 1982, 1100.
42 W. S. Kijlstra, D. S. Brands, H. I. Smit, E. K. Poels and A. Bliek, *J. Catal.*, 1997, **171**, 219–230.
43 Z. Wu, B. Jiang and Y. Liu, *Appl. Catal., B*, 2008, **79**, 347–355.
44 S. Andreoli, F. A. Deorsola, C. Galletti and R. Pirone, *Chem. Eng. J.*, 2015, **278**, 174–182.
45 K. M. Eid and H. Y. Ammar, *Appl. Surf. Sci.*, 2012, **258**, 7689–7698.
46 M. Breedon, M. J. S. Spencer and I. Yarovsky, *J. Phys. Chem. C*, 2010, **114**, 16603–16610.
47 N. N. Greenwood and A. Earnshaw, *Chemistry of the elements*, Butterworth-Heinemann, Oxford, 2nd edn, 1997, p. 1700.

